Research Square

Preprints are preliminary reports that have not undergone peer review.
They should not be considered conclusive, used to inform clinical practice,
or referenced by the media as validated information.

Development of a chronic rat model of perianal fistulizing Crohn's disease

Kai Ma
Yaqi Liao
Yikun Li
Yin Lu
Yibo Yao
Chen Wang
wangchen_longhua@163.com

Article

Keywords: perianal fistulizing Crohn's disease, Animal model, Intestinal inflammation, Multimodal assessment

Posted Date: September 23rd, 2026

DOI: https://doi.org/10.21203/rs.3.rs-10854567/v1

License: This work is licensed under a Creative Commons Attribution 4.0 International License.
Read Full License

Additional Declarations: No competing interests reported.

Abstract

Objective

Perianal fistulizing Crohn's disease (pfCD) is a common and debilitating complication of Crohn's disease for which clinically relevant and reproducible experimental models remain limited. This study aimed to develop and characterize a stable rat model that recapitulates key features of human pfCD.

Methods

Chronic colitis was induced in rats by repeated administration of 2,4,6-trinitrobenzene sulfonic acid (TNBS). A fistulous tract was subsequently created using a 2-mm-diameter steel wire, followed by local TNBS instillation to sustain fistula-associated inflammation. Model establishment was evaluated by colonoscopy, perineal ultrasonography (PU), and magnetic resonance imaging (MRI). Histopathological and molecular characterization included hematoxylin and eosin (H&E) staining, Alcian blue-periodic acid–Schiff (AB-PAS) staining, immunofluorescence, and Western blotting for intestinal barrier-associated proteins, including MUC2, ZO-1, and Occludin. Serum and colonic levels of IL-23, IL-12, TNF-α, and neutrophil gelatinase-associated lipocalin (NGAL) were measured by ELISA. Fistula-associated inflammatory features were further compared with fistula specimens obtained from 10 treatment-naïve patients with pfCD.

Results

Rats subjected to the two-stage induction protocol developed persistent clinical and endoscopic features of chronic colitis. Colonoscopy demonstrated mucosal erosions and ulceration accompanied by hyperemia and edema, while histological examination revealed marked mucosal injury and disruption of intestinal barrier integrity. Expression of MUC2, ZO-1, and Occludin was reduced, whereas serum and colonic levels of IL-23, IL-12, TNF-α, and NGAL were significantly increased ($P < 0.01$). Both PU and MRI confirmed the formation of persistent fistulous tracts. Immunofluorescence further demonstrated increased CD86 and MPO expression within fistula tissues of the rat model, with spatial expression patterns similar to those observed in fistula specimens from treatment-naïve patients with pfCD.

Conclusion

We developed a reproducible chronic rat model of pfCD using a two-stage induction strategy combining chronic TNBS-induced colitis with mechanically created and locally inflamed fistulous tracts. The model reproduces key endoscopic, imaging, histopathological, inflammatory, and barrier-associated features of human pfCD and may provide a useful preclinical platform for investigating disease mechanisms and evaluating therapeutic interventions.

Introduction

Crohn's disease (CD) is a chronic nonspecific inflammatory bowel disease characterized by transmural inflammation that predominantly affects the colorectal mucosa, though its precise etiology and pathogenesis remain elusive [1]. Epidemiological data from European populations reveal an annual incidence rate of approximately 12.7 per 100,000 individuals, notably, the incidence of CD in China has risen rapidly in recent years [2]. CD is characterized by a segmental and transmural inflammatory response throughout the entire digestive tract, which can easily infiltrate into adjacent organs, tissues, or the skin [3]. Epidemiological evidence indicates that approximately 45% of CD patients develop perianal complications, among them, perianal fistulizing Crohn's disease (pfCD) has become a major challenge in clinical management due to its high incidence, refractoriness, and high recurrence rate, imposing a substantial economic and psychological burden on their families [4–5].

The precise pathological mechanisms underlying pfCD remain incompletely elucidated. but it is mainly related to genetic, immune, environmental and intestinal microbial factors [6]. These factors jointly promote the continuous progression of transmural intestinal inflammation, ultimately resulting in the formation of characteristic fistula tracts [7]. Although recent advances in biologic agents and stem cell-based therapies have shown promise for some patients with pfCD, therapeutic efficacy remains constrained by disease heterogeneity and the absence of personalized treatment strategies [8–9]. This clinical challenge is partially rooted in the limitations of current animal models to replicate the complex pathophysiology of human pfCD, particularly their inability to recapitulate the dynamic "transmural inflammation-sinus tract formation-fibrosis" continuum that defines pfCD progression [10]. Therefore, establishing a reliable animal model that accurately mirrors the pathophysiological features of human pfCD is crucial for further elucidating its pathogenesis and facilitating the development of novel targeted therapies.

In recent years, 2,4,6-Trinitrobenzenesulfonic acid (TNBS) has attracted attention due to its unique immune activation properties. As a haptenic compound, TNBS can be dissolved in ethanol and administered to induce antigen-specific immune responses via covalent binding to intestinal proteins [11]. This process triggers the infiltration of $CD4^{+}$T cells, neutrophils, and macrophages, leading to transmural inflammation and longitudinally progressive bowel wall injury [12]. During the chronic phase of inflammation, it promotes the formation of granulomatous lesions and sustains a dysregulated immune microenvironment, predominantly driving Th1/Th17-type immune responses [13–14]. As such, the TNBS-induced model is regarded as one of the most pathologically relevant chemical models for CD. Nevertheless, systematic methodologies for establishing a model of perianal fistula complicating chronic intestinal inflammation—specifically, pfCD—remain underexplored.

Based on this, the present study innovatively proposes a two-phase induction strategy for establishing a novel rat animal model of pfCD: first, a chronic intestinal inflammatory background is established via periodic administration of TNBS to simulate the persistent immune dysregulation characteristic of CD.

Subsequently, secondary intervention through localized mechanical injury is applied to promote inflammatory invasion into perianal tissues and drive the epithelialization process of fistulas. Grounded in the clinicopathological features of pfCD, this study aims to develop a novel compound-induced animal model. By optimizing localized inflammatory induction and employing multimodal evaluation, we systematically validate the model's similarity to human disease in terms of anatomical structure, pathological progression, and molecular characteristics. The establishment of this model will not only contribute to elucidating the pathogenesis of pfCD but also provide a reliable preclinical platform for the development of novel biologics, localized drug delivery systems, and surgical intervention techniques, thereby advancing the progress of personalized treatment strategies.

Materials and methods

Materials

2,4,6-Trinitrobenzenesulfonic acid solution (TNBS, 5%W/V) was purchased from Dalian Meilun Biotechnology Company (Dalian, China). ELISA kit for detecting cytokines (IL-23, IL-12, TNF-α, and NGAL) was purchased from MLBIO (Shanghai, China). The primary antibodies against Occludin (91131), and CD86 (76755) were from Cell Signaling Technology (Danvers, MA, USA). ZO-1 (ab96587), MUC2 (ab272692), MPO (ab208670), and GAPDH (ab181602) were from purchased from Abcam (Cambridge, MA, USA). Alcian blue periodic acid schiff (AB-PAS) Stain kit was bought from Solarbio (Beijing, China). Hematoxylin and eosin (H&E) kit was obtained from Beyotime Institute of Biotechnology (Jiangsu, China). PVDF membranes were purchased from Millipore (Burlington, United States).

Patient selection.

A total of 10 patients with new-onset pfCD were enrolled from the Department of Proctology at Longhua Hospital, Shanghai University of Traditional Chinese Medicine, between June 2024 and March 2025. The identification of pfCD adhered to recognized consensus standards, relying on integrated assessment of clinical parameters, radiological appearances, laboratory markers, endoscopic characteristics, and histological examination [15]. Demographic and clinical characteristics were recorded for all participants, including age, sex, weight, BMI, smoking status, comorbidities, perianal Disease Activity Index (PDAI), Crohn's Disease Activity Index (CDAI), age at disease onset, disease location, disease duration, medication history, prior/current therapies, fistula characteristics (number), and endoscopic/radiographic assessment data. Serum and fecal inflammatory biomarkers—specifically Neutrophil gelatinase associated lipocalin (NGAL, reference interval: < 150 μg/L), fecal calprotectin (FC, reference interval: < 60 μg/g), C-reactive protein (CRP, reference interval: < 5 mg/L), and erythrocyte sedimentation rate (reference interval:<ESR 21 mm/h)—were quantitatively assessed. Standardized surgical intervention was performed on all enrolled patients with pfCD. Intraoperatively acquired fistula tract specimens were cryopreserved at -80°C within 30 minutes of excision to ensure biomolecular stability, facilitating subsequent histopathological and molecular analyses. To assess disease severity, the PDAI and CDAI were utilized. The CDAI yields a total score ranging from 0 to 600, where higher

scores indicate greater disease severity. disease activity is categorized as follows: remission (< 150), mild (150–220), moderate (221–450), and severe (> 450). Regarding the PDAI, it assesses five clinical domains: discharge, pain/activity limitation, restriction of sexual activity, type of perianal lesion, and severity of induration. The total PDAI score ranges from 0 to 20, with a score ≤ 4 indicating inactive disease and a score > 4 defining active fistulizing disease.

The study involving human participants was approved by the Institutional Review Board of Longhua Hospital, Shanghai University of Traditional Chinese Medicine (approval no. 2020LCSY032). All research involving human participants was performed in accordance with the relevant institutional and national guidelines and regulations and with the Declaration of Helsinki. Written informed consent was obtained from all adult participants before participation. For the participant who was a minor, written informed consent for study participation was obtained from a parent and/or legal guardian.

Inclusion and exclusion criteria.

Participants with PFCD were enrolled based on the following criteria: (a) a confirmed diagnosis of PFCD established through comprehensive clinical evaluation supplemented by endoscopic, histopathological, and/or magnetic resonance imaging (MRI) findings, along with relevant biochemical markers; (b) presence of at least one actively draining perianal fistula tract. Exclusion criteria included: (a) Concurrent anal strictures or untreated abscesses requiring emergent surgical drainage; (b) Secondary fistulas attributed to malignancies, traumatic injuries, or human immunodeficiency virus (HIV) infection; (c) Active gastrointestinal infections (e.g., bacterial/viral gastroenteritis); (d) history of major trauma or surgery within the preceding three months.

Experimental animals

Male Sprague Dawley rats (300 to 320 g) were purchased from Shanghai SLAC Laboratory Animal Co., Ltd. and housed in the Experiment Animal Center of Shanghai University of Traditional Chinese Medicine. The rats were housed in specific pathogen-free environments and kept under standard laboratory settings. Rats were unrestricted to obtain normal diet and water and housed under standard surroundings: temperature (20 ± 2 ℃), humidness (50 ± 10%), and illumination (12/12 h bright/dark cycles). This study was approved by the Animal Ethics Committee of Shanghai University of Traditional Chinese Medicine (license No. PZSHUTCM2503170017). The experimental design and animal use strictly adhered to the ethical principles of experimental animal welfare. The rats were housed individually in separate cages and provided with an adequate supply of water and food. In the stage of pre-experimentation, all rats were subjected to adaptive feeding for four weeks before the experiment.

Establishment of pfCD in a rat model

After 4 weeks of adaptive feeding, 10 healthy male Sprague Dawley rats (400-420g) were randomly divided into control group (Con, n = 5) and model group (Mod, n = 5). Colitis was induced by TNBS

according to a previously described method. TNBS 50 mg/kg, which was dissolved in ethanol 50% (the total volume of solution reached 1 mL) and was used for induction of CD. The model group was subjected to chronic colitis induction via alternating rectal enemas of TNBS and sterile saline (twice weekly for 6 weeks). A TNBS solution was prepared. Subsequently, with a polypropylene flexible catheter with an outer diameter of 2 mm. The lubricated tube was smoothly inserted into the colon 8 cm and TNBS slowly was injected by gavage needle 2–3 inches in length. After the TNBS injection, the rats were held in a vertical position for 5 minutes to avoid the outflow of the solution. The control group received the equal amount of the solvent. Subsequently, a 2 mm diameter steel wire was inserted at the 9 o'clock position (approximately 1 cm from the anal verge) in the lithotomy position to create a fistula tract. The fistula was then irrigated twice weekly with the TNBS (50 mg/kg, in 50% ethanol; twice weekly for 3 weeks), while TNBS enemas were continued throughout the study. General conditions, including hematochezia and food intake, were monitored. Body weight changes and disease activity index (DAI) were recorded every 3 days. At the experimental endpoint, rats were euthanized by an overdose of inhaled isoflurane. Each animal was placed individually in an induction chamber and exposed to 5% (v/v) isoflurane until deep anesthesia was achieved, followed by complete cessation of spontaneous respiration. Isoflurane exposure was maintained after respiratory arrest until death was confirmed. Death was verified by the absence of spontaneous respiration, cardiac activity, corneal reflex, and pedal withdrawal reflex. Only after confirmation of death were blood, colon, and perianal fistula tissues collected for subsequent analyses (Fig. 1).

Disease activity index (DAI) score

The rats were weighed and recorded every 3 days for 9 weeks. At the same time, the feces of pfCD rats were observed, the weight change, fecal characteristics and fecal bleeding of pfCD rats were considered, and the DAI score was determined. DAI = (body mass index + stool shape + bleeding)/3 [16]. (Table 1).

Table 1
Disease activity index scoring criteria.

Score	Loss of weight (%)	Stool consistency	Stool occult blood
0	None	Normal	Normal
1	1–5	loose stool	hidden blood positive
2	6–10	diarrhea	slight bloody stool
3	12–20	mild diarrhea	gross bloody stool
4	≥ 20	Watery diarrhea	Gross bleeding

HE Staining of the colon

HE staining was performed as previously described by RoseMarine et al, with minor modifications. Briefly, colon samples were fixed in 4% paraformaldehyde for 24 h, paraffin-embedded, and sectioned at 3 μM. Sections were stained with a commercial HE kit (Beyotime Institute of Biotechnology, Jiangsu, China) and examined by light microscopy (Olympus, Japan). Histological injury was scored by an investigator blinded to group allocation on the basis of inflammatory-cell infiltration, depth of tissue involvement, crypt architecture, and related histopathological features. [17]

Alcian Blue-Periodic Acid-Schiff Staining

To detect the mucous thickness and mucin-secreting goblet cells number count, AB-PAS staining was performed. AB-PAS (G1285, solarbio) staining kits were applied to the sectioned tissue slides following the manufacturers' recommended protocols. The prepared slides were examined under an upright optical microscope, and images were analyzed and quantified using Image-Pro Plus software.

Enzyme-linked immunosorbent assay (ELISA)

Concentrations of IL-23, IL-12, TNF-α, and NGAL in serum and colonic tissue lysates were quantified using commercial rat ELISA kits (MLBIO, Shanghai, China) in accordance with the manufacturer's instructions. For tissue analysis, 1 g of colon was homogenized in 10 mL ice-cold RIPA lysis buffer and centrifuged at 13,000 rpm for 30 min at 4°C. The clarified supernatant was used for the assay. Following the kit-specific incubation, washing, chromogenic-reaction, and stop-reaction steps, absorbance was measured at 450 nm using a microplate reader.

Immunofluorescence staining

The colon and fistula tissues were embedded into the optimal cutting temperature compound (TissueTek®, Tokyo, Japan) and stored at -80℃. Frozen specimens were cut into 5 μ m sections. Antigens were extracted using a solution containing citric acid for antigen repair. The sections were incubated with 5% BSA for 1 h to block nonspecific binding activity, and then incubated with primary antibody against ZO-1(1:500; Abcam), Occludin (1:500; CST), MUC2(1:500; Abcam), CD86(1:500; CST), and MPO (1:500; Abcam) at 4℃ overnight. Further experiments were carried out the next day, DAPI staining was performed to visualize the nuclei. After immunostaining, the slides was observed by fluorescence microscopy (Leica DM IRB; Leica, Wetzlar, Germany). Quantification of the intensity of the fluorescence colon and fistula section was performed by Image-Pro Plus 7.0 software (Media Cybernetics, Silver Spring, MD, USA).

Western blot analysis

Total protein was extracted from colon tissue using the RIPA lysis buffer, and quantified with the BCA kit (manufactured by Beyotime, China). SDS-PAGE was used for protein separation, and the wet transfer

method was used to transfer the protein to PVDF membranes. The protein was sealed with 5% BSA (bovine serum albumin) for 1 h at room temperature. The first antibody was added, including anti-ZO-1 (1:1000), anti-Occludin (1:1000), and anti-GAPDH (1:1000), and incubated overnight at 4℃. After washing the membrane three times, HRP-labeled sheep anti-rabbit secondary antibody (1:5000) was added and incubated at room temperature for 2 h at room temperature. After cleaning the film, the PVDF film was placed in the chemiluminescence system using an ECL assay kit for detection, analyzed by Image J software, and the relative protein expression level was calculated with reference to the expression of GAPDH.

Perianal ultrasound assessment

Low-dose isoflurane was used to anesthetize the experimental animals, with 3.5% for induction and less than 1% for maintenance. Then, the animals were immobilized in left lateral decubitus position on a platform where the temperature could be regulated.

All pfCD rats model underwent perianal ultrasound that were performed by a highly qualified radiologist with 10 years experience in general ultrasound imaging. The fistula was performed using a high-frequency ultrasound system (Vevo 2100; VisualSonics, Toronto, Canada) at the Experimental Animal Center of Shanghai University of Traditional Chinese Medicine. In the ultrasound images, the fistular tract appears as a tubular hypoechoic structure starting from the anal canal and extended to the perianal skin.

MRI scanning of fistulas

In this experiment, low-dose isoflurane was used to anesthetize the experimental animals. Specifically, the induction dose was set at 3.5%, and the maintenance dose was kept below 1%. After anesthesia, the animals were placed in a prone position on a temperature-controlled surgical platform and immobilized. Special attention was paid to firmly fixing the rat's buttocks to avoid any motion-induced artifacts. The Magnetic Resonance (MR) images were obtained using an 11.7T system from Bruker Biospin MRI GmbH in Ettlingen, Germany. To guarantee the accuracy of data collection, standard procedures were strictly adhered to. This involved calibrating the reference frequency power and adjusting the shim gradients with the MapShim function in Paravision v6.1. Axial T2-weighted imaging was carried out using a rapid acquisition of relaxation enhancement (RARE) sequence. The specific parameters were as follows: the repetition time (TR) was set at 120 ms, the echo time (TE) was 2.3 ms, the slice thickness was 0.5 mm, the number of slices was 30, the field of view (FOV) measured 18×18 mm^2, and the matrix size was 256×256. A single-shot echo-planar imaging (EPI) sequence was then implemented. The parameters for this sequence were: TR = 2000 ms, TE = 11.32ms, the flip angle was 90°, the slice thickness was 0.5 mm, the number of slices was 30, the FOV was 18×18 mm^2, the matrix size was 90×90, and the number of volumes was 240. For the diffusion tensor imaging (DTI) acquisition, the protocol parameters were as follows: TR was 2500 ms, TE was 18 ms, the number of excitations (NEX) was 1, the FOV was 18×18 mm^2, the matrix size was 180×180, the number of slices was 30, and the anisotropic voxel resolution was 0.1×0.1×0.5 mm^3.

Statistical analysis

Data analyses were performed using GraphPad Prism 9.5 (GraphPad Software, USA). Statistical analyses were carried out with SPSS (Version 26.0, IBM, United States). The Shapiro-Wilk test was employed to evaluate the data distribution. Measurement data with normal distribution were expressed as mean ± standard deviation (M ± SD) and analyzed between groups using the t-test. Non-normally distributed variables were presented as median and interquartile range (IQR) and the Mann-Whitney rank -sum test was applied for comparison. Differences were considered statistically significant at $P < 0.05$, ** $P < 0.001$.

Results

1.1 Patient characteristics.

The pfCD group exhibited significantly elevated levels of NGAL, FC, CRP, and ESR compared to established reference ranges. In terms of age stratification, Group A1 (< 17 years) included 1 case (10.0%); Group A2 (17–40 years) had 7 cases (70.0%); and Group A3 (> 40 years) consisted of 2 cases (20.0%); Regarding disease localization, 2 patients (20.0%) had L1 (isolated ileal) involvement, 2 (20.0%) had L2 (colonic only), and 6 (60.0%) had L3 (ileocolonic) disease; For behavioral phenotypes, 7 patients (70.0%) presented with B1 (inflammatory/non-stricturing), 3 (30.0%) had B2 (stricturing), and no cases of B3 (penetrating) were observed according to the Montreal classification system. The detailed demographic and clinical characteristics are presented in Supplementary Table 1.

1.2 Model assessment

The control group rats exhibited progressive weight gain, normal feeding behavior, and locomotor agility. After 6 weeks of inducing chronic colitis in the rats demonstrated characteristic disease manifestations including graded loose stools, macroscopic hematochezia, appetite suppression, psychomotor retardation, and affective flattening. The body weight of the rats in the model group gradually decreased over time, and the DAI score increased with the time (Fig. 2B, C). The seton was removed 3 weeks after the anal fistula modeling, purulent discharge from the external fistula after steel wire removal (Fig. 2A-d). One week later, the external opening of the fistula did not close (Fig. 2A-e, f), indicated that fistulas have matured and did not have the tendency for spontaneous healing, which demonstrated the persistent inflammatory state within the fistula.

1.3 Pathological Features of Intestinal Inflammation in Rats model of pfCD

Histological examination demonstrated a clear contrast between the two groups. Colonic sections from control rats showed preserved mucosal architecture, with intact epithelial, muscularis mucosae, submucosal, and muscular layers, regularly organized crypts, and abundant goblet cells. In the model group, the normal layered architecture was markedly disrupted. Extensive mucosal epithelial loss and necrosis, crypt depletion, pronounced bowel-wall thickening, dense inflammatory-cell infiltration, vascular congestion, edema, and ulceration were observed (Fig. 3B). AB-PAS staining further demonstrated abundant goblet cells and preserved mucin production in controls, whereas model

animals showed a substantial reduction in goblet-cell abundance and mucin staining (Fig. 3B, D). Consistent with these histological findings, immunofluorescence showed lower MUC2 expression and higher CD86 staining in the model group than in controls, with statistically significant between-group differences (Fig. 3C, E).

1.4 Expression of intestinal barrier protein

Immunofluorescence results revealed that in the colon tissues of the control group, the ZO-1 and Occludin proteins were mainly localized at the tight junctions of intestinal epithelial cells, presenting clear and continuous positive staining, suggesting the integrity of the intestinal barrier structure. However, the positive staining of ZO-1 and Occludin proteins was significantly weakened in the model group (Fig. 4-A, C). The Western blot results shown that, compared with the control group, the protein expression of ZO-1 and Occludin protein was significantly decreased in the model group (Fig. 4-B, D, E) ($P < 0.001$).

1.5 Expression level of inflammatory factor between the two groups.

To determine the roles of TNBS in regulating the inflammation levels, we thus examined the levels of various inflammatory cytokines in both serum and colon tissues. As shown in Fig. 5, the expression of the proinflammatory cytokines IL-23, IL-12, TNF-α and NGAL was significantly increased, suggesting the baseline alterations in the systemic inflammation following the stimulation of TNBS.

1.6 Imaging Evaluation of Perianal Fistulas

PU provides real-time, high-resolution visualization of superficial fistula tracts and surrounding structures. In pfCD rat models, fistulas typically manifest as hypoechoic linear or tubular structures originating from the external opening of the fistula and extending to the anorectal wall, often accompanied by irregularly shaped hyperechoic foci representing fibrosis or gas pockets (Fig. 6-A). Perianal MRI provides a more comprehensive and detailed view of the perianal fistula in rats with pfCD compared to perianal ultrasound. It can clearly show the entire course of the fistula tract, as well as its relationship with the surrounding anatomical structures. Through MRI examination of the rat model of pfCD, visible fistulas were found in all 5 experimental rats (100%), with both internal and external openings clearly observable. MRI demonstrated the external opening, tract course, and internal opening of the fistula, as well as the extent of the abscess, utilizing axial fat-suppressed T2-weighted imaging (T2WI-FS) as the foundational sequence. On T2WI-FS sequences, the fistula tract appears as a high-signal intensity tubular structure, which is due to the presence of fluid or inflammatory exudate within the tract. (Fig. 6-B).

1.7 Comparative histopathological and immunofluorescence analysis of perianal fistula tissues from clinical pfCD patients and experimental pfCD rat models.

Through HE staining and immunofluorescence staining techniques, we systematically compared key histopathological characteristics of anal fistula tissues from clinical pfCD patients and those from an

established rat model of pfCD. The Longitudinal and cross-sectional views with HE staining results showed that in clinical patients, the perianal fistula tissues exhibited diffuse inflammatory cell infiltration with patchy or focal aggregation patterns, accompanied by localized tissue necrosis and liquefaction forming variably sized cavities. Loose granulation tissue proliferation was observed around the lesions. Consistently, the pfCD rat model demonstrated analogous histomorphological characteristics, including comparable patterns of inflammatory cell infiltration, localized tissue destruction, and granulation tissue hyperplasia. These parallel findings indicate that a high degree of similarity in histomorphological structure between clinical and experimental groups (Fig. 7e-h, m-p).

Consistently, the Immunofluorescence staining further demonstrated that CD86-positive macrophages and MPO-positive neutrophils were detected in the perianal fistula tissues of both clinical patients and pfCD rat models, these immune cells were mainly distributed in the inflammatory infiltration areas and tissue around the fistulas, showing a scattered or clustered distribution, and with no statistically significant differences observed between the experimental and clinical cohort. This finding indicates a high degree of consistency in the infiltration of specific immune cells between the two groups, which verifies the applicability of this rat model as a reliable tool for studying human pfCD (Fig. 7-i-l, q-t). Further details on nine pfCD cases and four experimental pfCD rat models are provided in the Supplementary Material.

Discussion

pfCD represents a severe and challenging complication of Crohn's disease, characterized by its refractory and recurrent nature, which imposes a substantial socioeconomic burden on the general population [18]. To advance our understanding of fistula pathogenesis and facilitate the development of novel targeted therapies, the establishment of reliable preclinical models replicating the pathophysiological features of human pfCD remains a critical prerequisite for both mechanistic exploration and therapeutic innovation [19]. This hierarchical and progressive modeling approach not only recapitulates the clinicopathological progression from chronic inflammation to structural destruction observed in pfCD, but also enables precise modulation of inflammatory intensity and fibrotic severity through TNBS concentration optimization and dosing interval adjustments, thereby creating essential conditions for fistula development. Through multimodal evaluations (including imaging, histopathological, and molecular biological analyses), we have successfully established a composite rat model of chronic CD complicated with perianal fistula.

Since Morris GP et al. first reported the establishment of experimental colitis in rats using TNBS in 1989, this model has been extensively employed in CD research [20]. The TNBS-induced intestinal inflammation model demonstrates histopathological features closely resembling human CD manifestations, including transmural inflammation, lymphocyte infiltration, and ulceration. Its technical simplicity and high reproducibility make it an ideal platform for investigating CD pathogenesis and therapeutic interventions [21]. Furthermore, by adjusting the induction period, the TNBS model can simulate different stages of CD: the acute phase is characterized predominantly by neutrophil infiltration and mucosal

ulceration, whereas the chronic phase involves lymphocyte aggregation, fibrosis, and transmural pathology. This dynamic progression makes it a suitable platform for studying the mechanisms of pfCD.

Previous studies have documented diverse approaches to modeling pfCD. Rivera-Nieves et al. established the SAMP1/YitFc spontaneous fistula mouse model, however, only 5% of the mice developed anal fistula lesions, which limited the application of this model in research [22]. Additionally, previous studies have reported that rabbits, pigs, and dogs can be used to construct pfCD models. Nevertheless, these animals are subject to certain limitations in terms of animal rearing, cost, body size, and reproducibility, rendering them suboptimal for pfCD research [23-25]. In this experiment, rats were selected as the experimental animals because of their moderate body size, which makes them easy to rear and handle [26]. Compared with large-sized animals, rats require less experimental space, facilitating large-scale experimental research in the laboratory. When administering TNBS via enema, the drug dosage and injection depth can be accurately controlled. The 12-o'clock position in the lithotomy position is close to the perineal body (containing the urethral and genital openings), and the operation at this position may easily damage the urethra. The 6-o'clock position is adjacent to the coccyx, and puncturing at this site may damage the coccygeal nerves or blood vessels, interfering with the experimental results. Therefore, placing a seton at the 9-o'clock in the lithotomy position can better mimic the common onset sites of human pfCD. It is also easy to locate and operate, with a relatively wide field of view, which is convenient for the entry of surgical instruments. During the experiment, it was found that after placing a common silk thread seton around the anus of rats, the rats would bite off the seton, affecting the formation of the fistula. Subsequently, by improving the experimental protocol, a 2 mm diameter steel wire seton was placed around the anus of rats, successfully inducing the establishment of an anal fistula model in rats.

Inflammatory factors play a central role in the pathogenesis of pfCD. The imbalance between pro-inflammatory and anti-inflammatory factors leads to a persistent inflammatory state [27]. IL-23, as an important pro-inflammatory cytokine, plays a crucial role in regulating the differentiation and function of T helper 17 (Th17) cells [28]. Its elevated expression in both serum and intestinal tissues of the model group indicates an active Th17-mediated immune response in the rat pfCD model. IL-12, primarily produced by antigen-presenting cells, it can promote the differentiation of Th1 cells and the secretion of interferon-γ (IFN-γ), and is extensively involved in inflammatory immune responses. Tumor necrosis factor-(TNF-α) is a pro-inflammatory cytokine with extensive biological activities, which plays an important role in the progression of the inflammatory response and immune regulation [29]. Neutrophil gelatinase-associated lipocalin (NGAL) is a protein closely related to inflammation and tissue damage. It reflects the degree of intestinal mucosal damage and inflammation in the pfCD model [30]. The significantly elevated levels of NGAL in the serum and tissues of the model group further confirm the important roles of intestinal barrier dysfunction and neutrophil activation in the formation of anal fistulas. These findings collectively demonstrate that the TNBS-induced rat model recapitulates immunopathological features highly consistent with those observed in clinical pfCD patients, which verifies that the TNBS-induced model successfully mimics the core pathological features of pfCD,

including the imbalance of Th1/Th17 immune responses, the cascade release of pro-inflammatory factors, and the tissue destruction mechanism mediated by neutrophil infiltration.

The intestinal barrier plays a critical role in maintaining intestinal homeostasis and preventing pathogen invasion. ZO-1 and Occludin, as essential components of tight junction proteins, are integral to the structural integrity of the intestinal physical barrier [31]. Downregulation of their expression reflects disruption of this barrier, which may lead to the abnormal penetration of luminal contents (such as bacteria and antigens), activate the innate immune system, and subsequently trigger a persistent inflammatory response. In addition, MUC2 is the main component of the intestinal mucosal mucus layer. A decrease in its expression may weaken the chemical defense function of the mucus barrier, making epithelial cells more vulnerable to the invasion of pathogens and inflammatory factors [32]. The dual damage to the intestinal barrier function (physical and chemical barriers) may be the key pathological basis for the continuous progression of tissue damage and chronic inflammation in the pfCD rat model. CD86, a co-stimulatory molecule primarily expressed on APC (such as macrophages and dendritic cells), exhibits upregulated expression in the model group, indicating significant local immune cell activation and enhanced antigen presentation function in the intestinal tissue [33]. There may be a mutually promoting relationship between intestinal barrier function disruption and inflammatory response in the occurrence and development of pfCD. Impairment of the intestinal barrier function allows antigenic substances in the intestinal lumen to more easily enter the intestinal mucosa, stimulating the activation of immune cells and triggering an inflammatory response. In turn, cytokines and inflammatory mediators produced during the inflammatory response can further damage intestinal epithelial cells and inhibit the expression of intestinal barrier proteins, leading to a further deterioration of the intestinal barrier function. This creates a vicious cycle of “barrier disruption-inflammation exacerbation-impaired barrier repair,” which may represent a critical mechanism underlying the refractory nature and high recurrence rate of pfCD.

For the evaluation of fistulas, perianal high-frequency ultrasound is initially employed to monitor the fistula tract, revealing hypoechoic fistula pathways and surrounding inflammatory edema zones. This is complemented by MRI findings, where T2-weighted hyperintense signals and rim-enhancement characteristics on contrast imaging provide synergistic diagnostic information [34-35]. The combined application of these two non-invasive imaging techniques not only improves the sensitivity of fistula recognition but also realizes a three-dimensional evaluation from morphological structure to functional status, providing an accurate positioning basis for subsequent pathological sampling. At the histopathological level, HE staining demonstrates extensive deposition of necrotic debris within the fistula tissue, accompanied by inflammatory cell infiltration, predominantly neutrophils and macrophages, within the fistula. Additionally, abnormal proliferation of newly formed capillaries is observed in the surrounding granulation tissue. This is consistent with the typical pathological changes in the active stage of human pfCD, suggesting that the continuous chemical stimulation induced by TNBS triggers a vicious cycle of necrosis-repair in local tissues. Furthermore, molecular pathological evidence elucidates the immunological basis of fistula formation. Through the co-localization of CD86 (a

macrophage marker) and MPO (a neutrophil marker) in the fistula tissue, it is revealed that the excessive activation of the innate immune system plays a pivotal role in the disease progression. Neutrophils contribute to oxidative stress via MPO release, compromising tissue structural integrity, while M1 macrophages persistently secrete pro-inflammatory cytokines such as TNF-α, fostering a chronic inflammatory microenvironment [36]. This spatial co-localization of immune cells may provide mechanistic insight into the refractory and recurrent clinical characteristics often observed in patients with pfCD.

The key innovations of our model are as follows: (1) The establishment of chronic intestinal inflammation via TNBS administration prior to fistula induction aims to recapitulate the pathological progression of CD, characterized by “inflammation-tissue destruction-fistula formation”; (2) The full-course administration of TNBS effectively mimics the characteristic of the recurrent and intractable course of CD; (3) The integration of cross-scale validation using imaging (ultrasound/MRI) and molecular pathology markers not only enhances the reliability of model evaluation but also closely mirrors the “imaging plus pathology” diagnostic approach routinely employed in clinical practice. However, this study acknowledges certain limitations that warrant further investigation. First, due to the limitations of the anatomical structure of rats, it is currently not possible to reproduce the clinical classification of pfCD in humans, such as inter‐sphincteric, trans‐sphincteric, supra‐sphincteric and extra‐sphincteric. Second, TNBS enema only mimics the inflammatory lesions in the rat colon and fails to form the characteristics of the whole digestive tract lesions of CD in clinical.

In conclusion, we developed a composite rat model of pfCD, the model can simulate the human condition, and the intestinal and fistula lesions induced can be evaluated by endoscopic, PU, MRI and histological examinations. The successful establishment of this model provides an experimental platform for both clinical and basic research on pfCD in the future.

Declarations

Clinical trial number

Not applicable.

Data Availability

Datasets of this work are available from the corresponding authors upon reasonable request.

Author Contributions

All authors contributed intellectually to the methodological framework and experimental architecture of this investigation. Specifically: Yibo Yao and Chen Wang were responsible for conceptualization and study design, and critically revised the manuscript for intellectual content; Kai Ma was responsible for the establishment of animal models and performed the experimental procedures, and prepared the

preliminary manuscript draft; Lu Yin was in charge of clinical case collection; Yikun Li and Yaqi Liao conducted the acquisition and analysis of imaging data. All authors reviewed and approved the final version of the manuscript.

Funding

This paper was published as part of a supplement financially supported by Shanghai Municipal Health Commission-Shanghai Sinus Fistula Disease Research Center (2023ZZ02003); Shanghai Hospital Development Center Foundation (SHDC22021316-A); Shanghai Hospital Development Center Foundation (SHDC22024306); National Administration of Traditional Chinese Medicine Key Discipline in High-Level TCM(ZYYZDXK-2023064); National Natural Science Foundation of China (82305237).

Disclosure

All authors declare they have no financial conflicts.

References

1. Dolinger, M., Torres, J. & Vermeire, S. Crohn's disease. *Lancet* **403** (10432), 1177–1191 (2024).
2. Lee, S. H. et al. Development and Validation of an Integrative Risk Score for Future Risk of Crohn's Disease in Healthy First-Degree Relatives: A Multicenter Prospective Cohort Study. *Gastroenterology* **168** (1), 150–153e4 (2025).
3. Mignini, I. et al. Fibrostenosing Crohn's Disease: Pathogenetic Mechanisms and New Therapeutic Horizons. *Int. J. Mol. Sci.* **25** (12), 6326 (2024).
4. Singh, A. et al. Management of Perianal Fistulizing Crohn's Disease. *Inflamm. Bowel Dis.* **30** (9), 1579–1603 (2024).
5. Gonczi, L. et al. Burden of perianal disease in Crohn's disease: Accelerating medical therapy and high rates of perianal surgery over the last four decades-Results from a population-based study over four decades. *Aliment. Pharmacol. Ther.* **59** (5), 656–665 (2024).
6. Cao, S., Colonna, M. & Deepak, P. Pathogenesis of Perianal Fistulising Crohn’s Disease: Current Knowledge, Gaps in Understanding, and Future Research Directions. *J. Crohns Colitis*. **17** (6), 1010–1022 (2023).
7. Parian, A. M. et al. Management of Perianal Crohn’s Disease. *Am. J. Gastroenterol.* **118** (8), 1323–1331 (2023).
8. Fudman, D. I. et al. Modern Advanced Therapies for Inflammatory Bowel Diseases: Practical Considerations and Positioning. *Clin. Gastroenterol. Hepatol.* **23** (3), 454–468 (2025).
9. Guillo, L. et al. Efficacy of mesenchymal stem cell-based therapies in the treatment of perianal fistulizing Crohn's disease: a systematic review and meta-analysis. *Stem Cell. Res. Ther.* **16** (1), 152 (2025).

10. Lu, S. et al. Evaluation of animal models of Crohn's disease with anal fistula (Review). *Exp. Ther. Med.* **22** (3), 974 (2021).
11. Katsandegwaza, B., Horsnell, W. & Smith, K. Inflammatory Bowel Disease: A Review of Pre-Clinical Murine Models of Human Disease. *Int. J. Mol. Sci.* **23** (16), 9344 (2022).
12. Yasuda, H. et al. Neutrophil extracellular trap induction through peptidylarginine deiminase 4 activity is involved in 2,4,6-trinitrobenzenesulfonic acid-induced colitis. *Naunyn Schmiedebergs Arch. Pharmacol.* **397** (5), 3127–3140 (2024).
13. Tang, J. et al. Huanglian Ejiao Decoction Alleviates Ulcerative Colitis in Mice Through Regulating the Gut Microbiota and Inhibiting the Ratio of Th1 and Th2 Cells. *Drug Des. Devel Ther.* **19**, 303–324 (2025).
14. Hu, Y. et al. Gegen Qinlian decoction ameliorates TNBS-induced ulcerative colitis by regulating Th2/Th1 and Tregs/Th17 cells balance, inhibiting NLRP3 inflammasome activation and reshaping gut microbiota. *J. Ethnopharmacol.* **328**, 117956 (2024).
15. Geldof, J. et al. Classifying perianal fistulising Crohn's disease: an expert consensus to guide decision-making in daily practice and clinical trials. *Lancet Gastroenterol. Hepatol.* **7** (6), 576–584 (2022).
16. Liu, M. H. et al. Therapeutic effect of Yiyi Fuzi Baijiang formula on TNBS-induced ulcerative colitis via metabolism and Th17/Treg cell balance. *J. Ethnopharmacol.* **309**, 116301 (2023).
17. Stillie, R. & Stadnyk, A. W. Role of TNF receptors, TNFR1 and TNFR2, in dextran sodium sulfate-induced colitis. *Inflamm. Bowel Dis.* **15** (10), 1515–1525 (2009).
18. Wong, S. Y. et al. Perianal Fistulizing Crohn's Disease-Associated Anorectal and Fistula Cancers: Systematic Review and Expert Consensus. *Clin. Gastroenterol. Hepatol.* **23** (6), 927–945e2 (2025).
19. Flacs, M. et al. Preclinical Model of Perianal Fistulizing Crohn's Disease. *Inflamm. Bowel Dis.* **26** (5), 687–696 (2020).
20. Morris, G. P. et al. Hapten-induced model of chronic inflammation and ulceration in the rat colon. *Gastroenterology* **96** (3), 795–803 (1989).
21. Fitzpatrick, L. R. et al. A new model of chronic hapten-induced colitis in young rats. *J. Pediatr. Gastroenterol. Nutr.* **50** (3), 240–250 (2010).
22. Rivera-Nieves, J. et al. Emergence of perianal fistulizing disease in the SAMP1/YitFc mouse, a spontaneous model of chronic ileitis. *Gastroenterology* **124** (4), 972–982 (2003).
23. Maldonado-Contreras, A. et al. Dysbiosis in a canine model of human fistulizing Crohn's disease. *Gut Microbes*. **12** (1), 1785246 (2020).
24. Lu, S. S. et al. Establishing a rabbit model of perianal fistulizing Crohn's disease. *World J. Gastroenterol.* **28** (15), 1536–1547 (2022).
25. Parian, A. M. et al. A Novel Patient-like Swine Model of Perianal Crohn's Disease. *Dis. Colon Rectum*. **66** (3), 425–433 (2023).

26. Li, L. et al. A nanofiber-hydrogel composite improves tissue repair in a rat model of Crohn's disease perianal fistulas. *Sci. Adv.* **9** (1), eade1067 (2023).
27. Panés, J. & Rimola, J. Perianal fistulizing Crohn's disease: pathogenesis, diagnosis and therapy. *Nat. Rev. Gastroenterol. Hepatol.* **14** (11), 652–664 (2017).
28. Korta, A., Kula, J. & Gomułka, K. The Role of IL-23 in the Pathogenesis and Therapy of Inflammatory Bowel Disease. *Int. J. Mol. Sci.* **24** (12), 10172 (2023).
29. Efrati, C. et al. Pathophysiology of Crohn's disease inflammation and recurrence. *Biol. Direct*. **15** (1), 23 (2020).
30. Romejko, K., Markowska, M. & Niemczyk, S. The Review of Current Knowledge on Neutrophil Gelatinase-Associated Lipocalin (NGAL). *Int. J. Mol. Sci.* **24** (13), 10470 (2023).
31. Chen, Y. et al. Interaction Between Commensal Bacteria, Immune Response and the Intestinal Barrier in Inflammatory Bowel Disease. *Front. Immunol.* **12**, 761981 (2021).
32. Qiao, Y. et al. Intestinal mucus barrier: A potential therapeutic target for IBD. *Autoimmun. Rev.* **24** (2), 103717 (2025).
33. Luo, M. et al. Macrophage polarization: an important role in inflammatory diseases. *Front. Immunol.* **15**, 1352946 (2024).
34. Zhang, H. et al. Development and validation of the MRI-based deep learning classifier for distinguishing perianal fistulizing Crohn's disease from cryptoglandular fistula: a multicenter cohort study. *EClinicalMedicine* **78**, 102940 (2024).
35. Hong, N. et al. Assessment of perianal fistulizing Crohn's disease activity with endoanal ultrasound: A retrospective cohort study. *World J. Gastrointest. Surg.* **16** (8), 2494–2502 (2024).
36. Wang, H., Huang, T. & Ma, Y. Mechanisms and therapeutic strategies of macrophages and neutrophils inducing ulcerative colitis progression. *Front. Immunol.* **16**, 1615340 (2025).

Figures

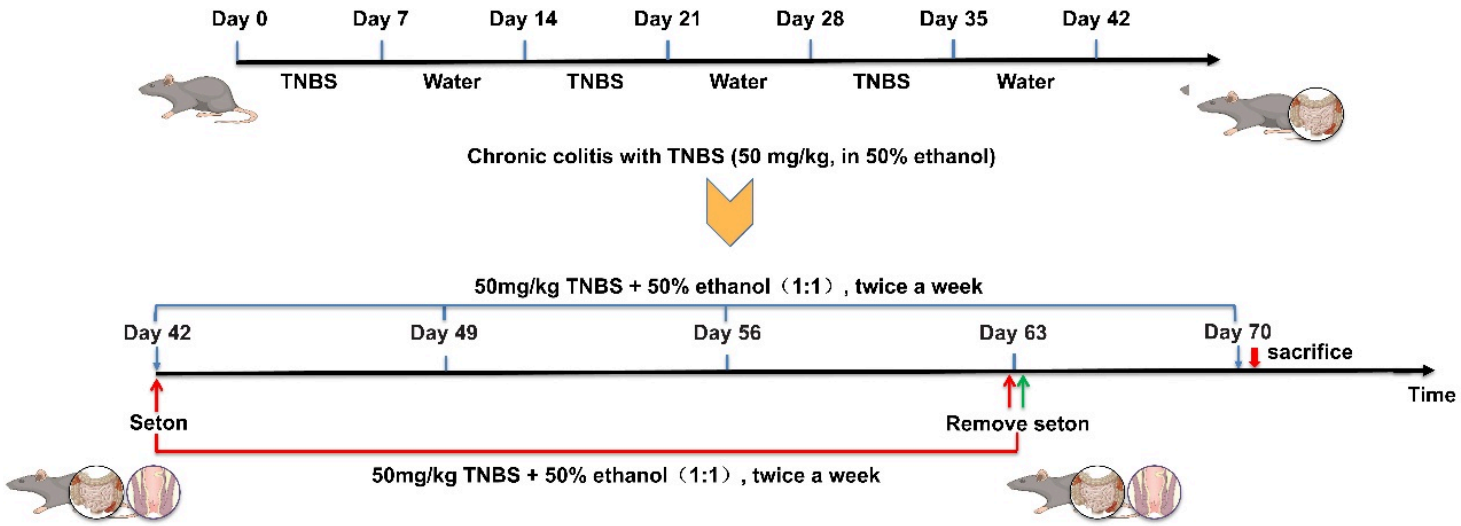


Figure 1

Flow chart of the rat pfCD model establishment protocol

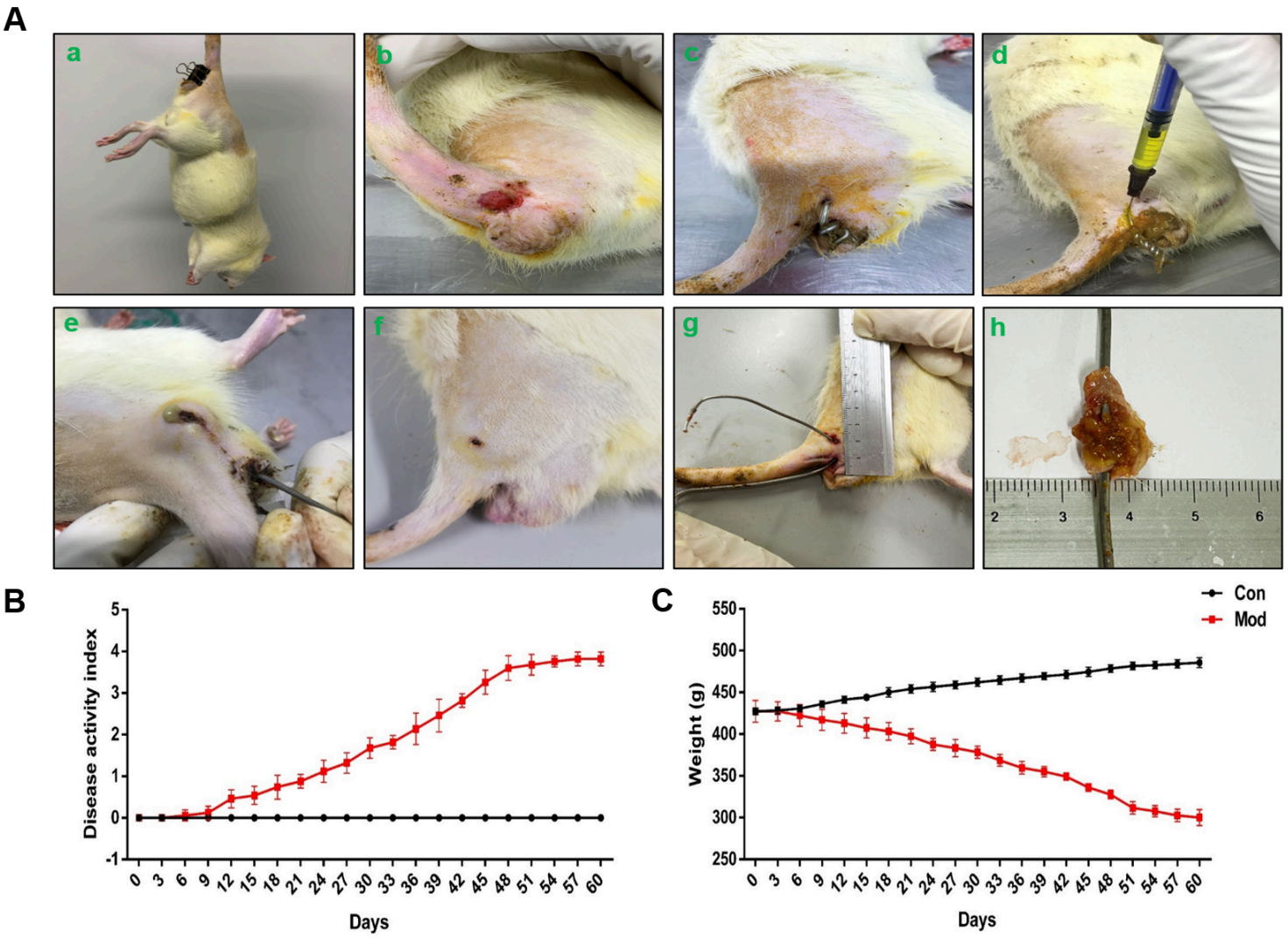


Figure 2

Assessment of experimental pfCD rat models. A: a: Rats were inverted for 3 minutes after enema; b: Bloody stool observed at rat anus; c: Perianal steel wire seton placement; d: TNBS injection; e: Purulent discharge from the external fistula after steel wire removal; f: Persistent patency of fistula tracts 1-week post-seton extraction; g: The fistula tract was pre-completely excised surgically; h: perianal fistula tissues. B, C: DAI scores and body weight changes of rats during TNBS treatment.

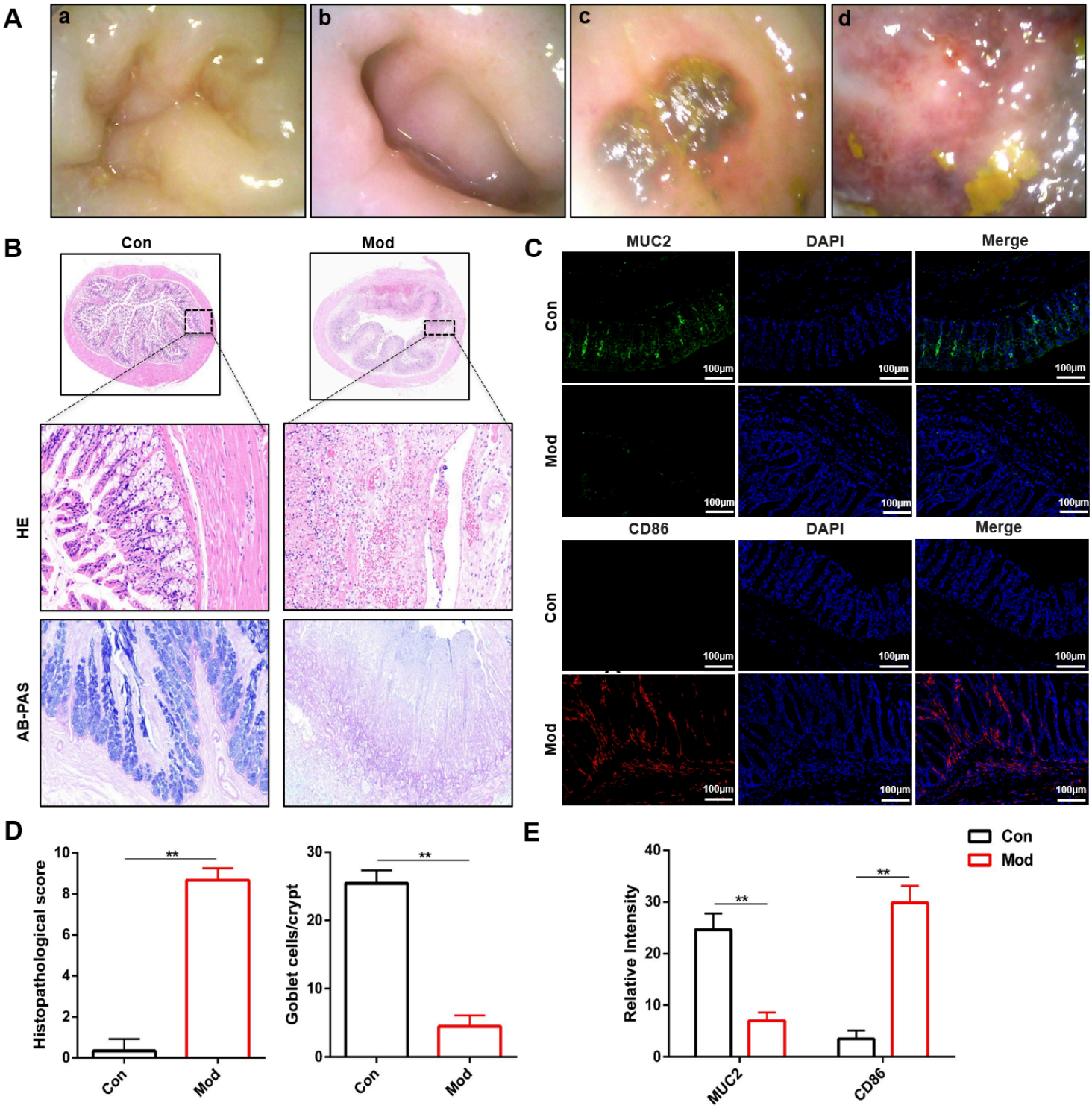


Figure 3

The characteristics of intestinal Inflammation in pfCD rats. A: a, b: Colonoscopy of control group; c, d: Colonoscopy of model group; B, D: Representative HE staining, AB-PAS staining images and quantitative analysis (20×). Scale bars, 50 μm. C, E: Representative Immunofluorescence staining and quantitative analysis (20×). Scale bars, 75 μm. *$P < 0.05$, **$P < 0.001$.

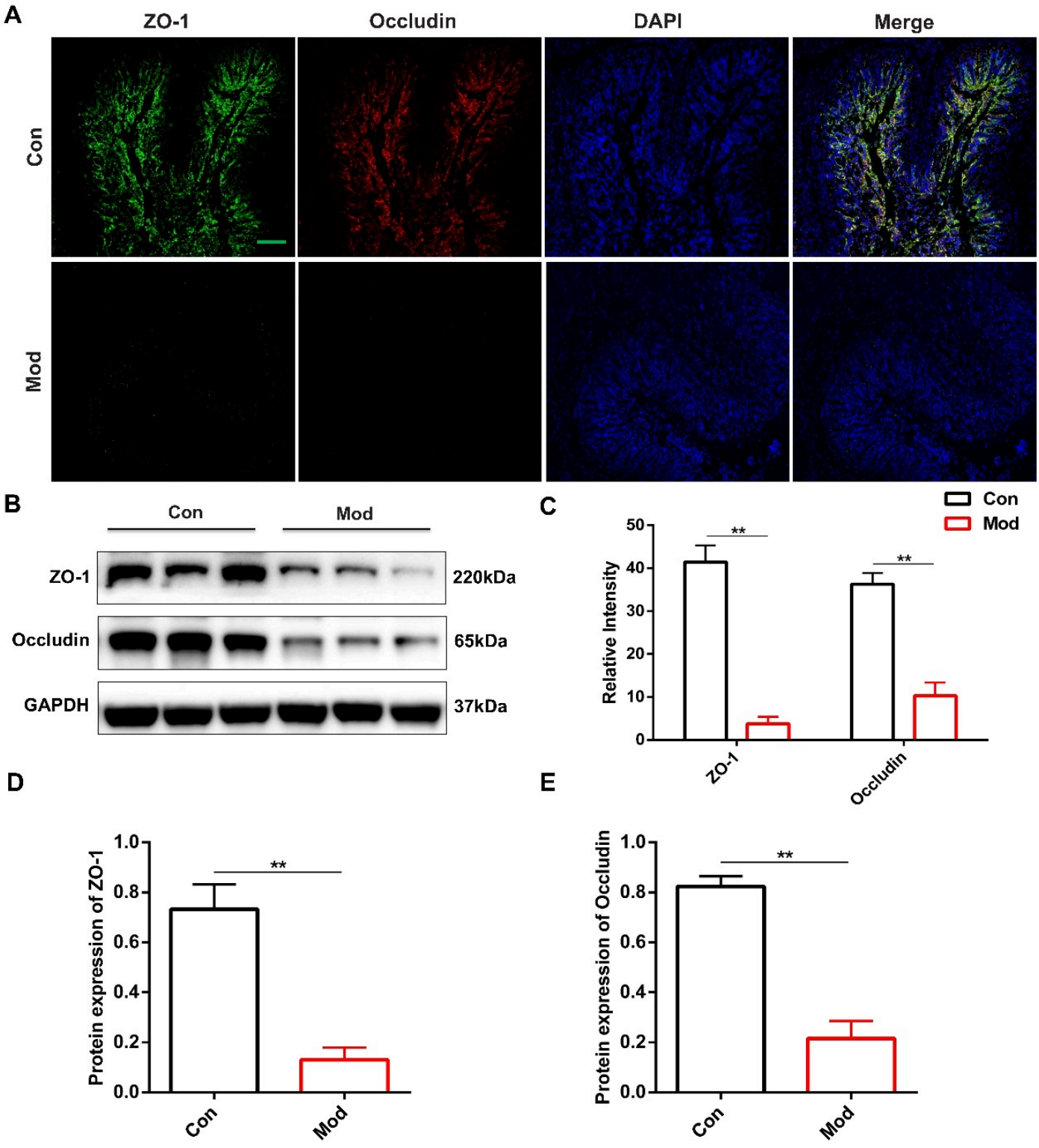


Figure 4

Expression of intestinal barrier proteins. A, C: Representative immunofluorescence staining and quantitative analysis of ZO-1 and Occludin (20×; scale bars, 100 μm). B, D, E: Representative cropped immunoblots and densitometric quantification of ZO-1 and Occludin, normalized to GAPDH. Cropping was performed only for presentation. Original, uncropped blots/gels, including membrane/gel edges and molecular-weight markers, are presented in Supplementary Figure S1. *$P < 0.05$, **$P < 0.001$.

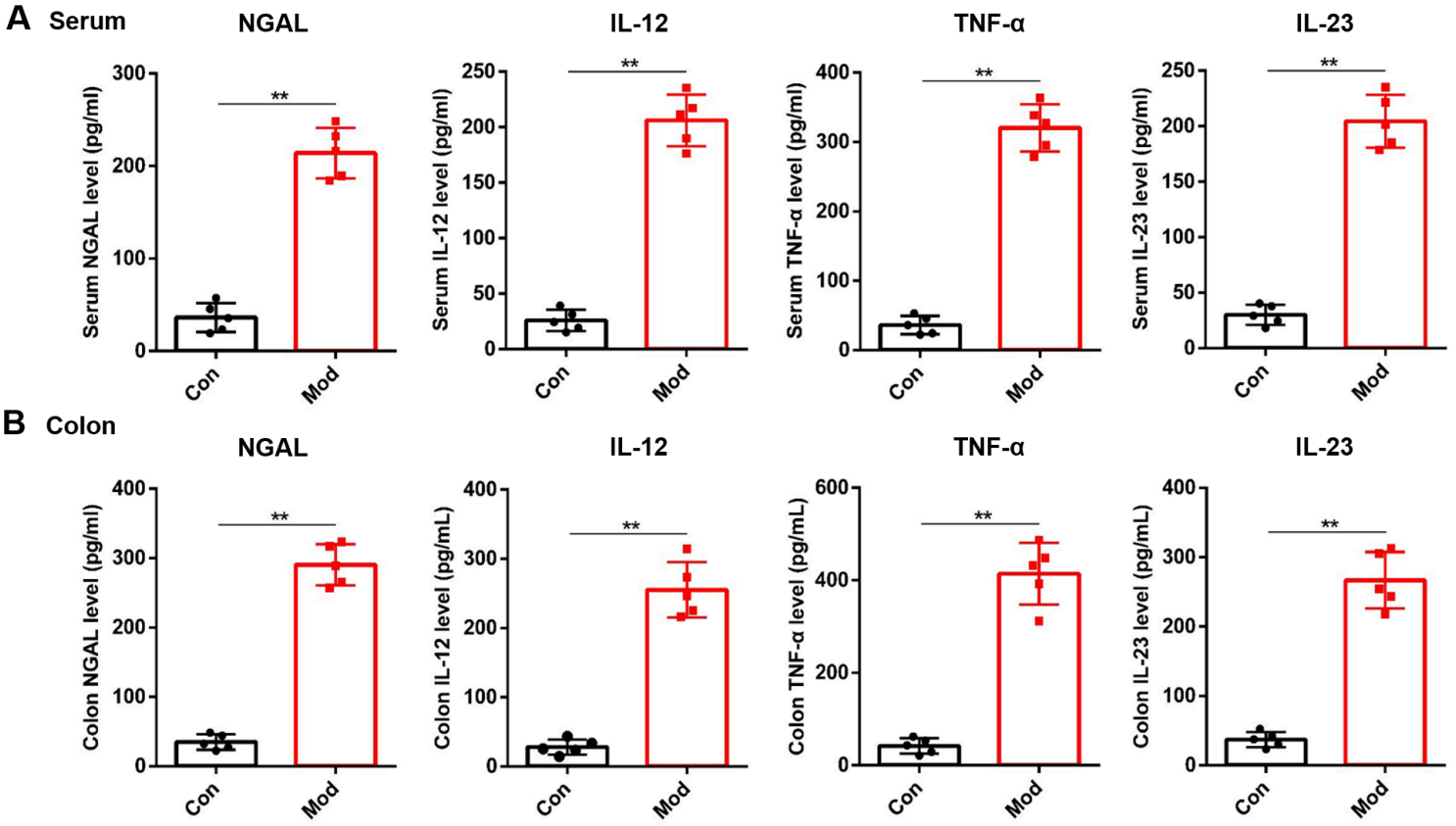


Figure 5

Expression level of inflammatory factor between the two groups. A: The expression levels of NGAL, IL-12, TNF-α, IL-23 in serum; B: The expression levels of NGAL, IL-12, TNF-α, IL-23 in colon tissues. *P < 0.05, **P < 0.001, n=5.

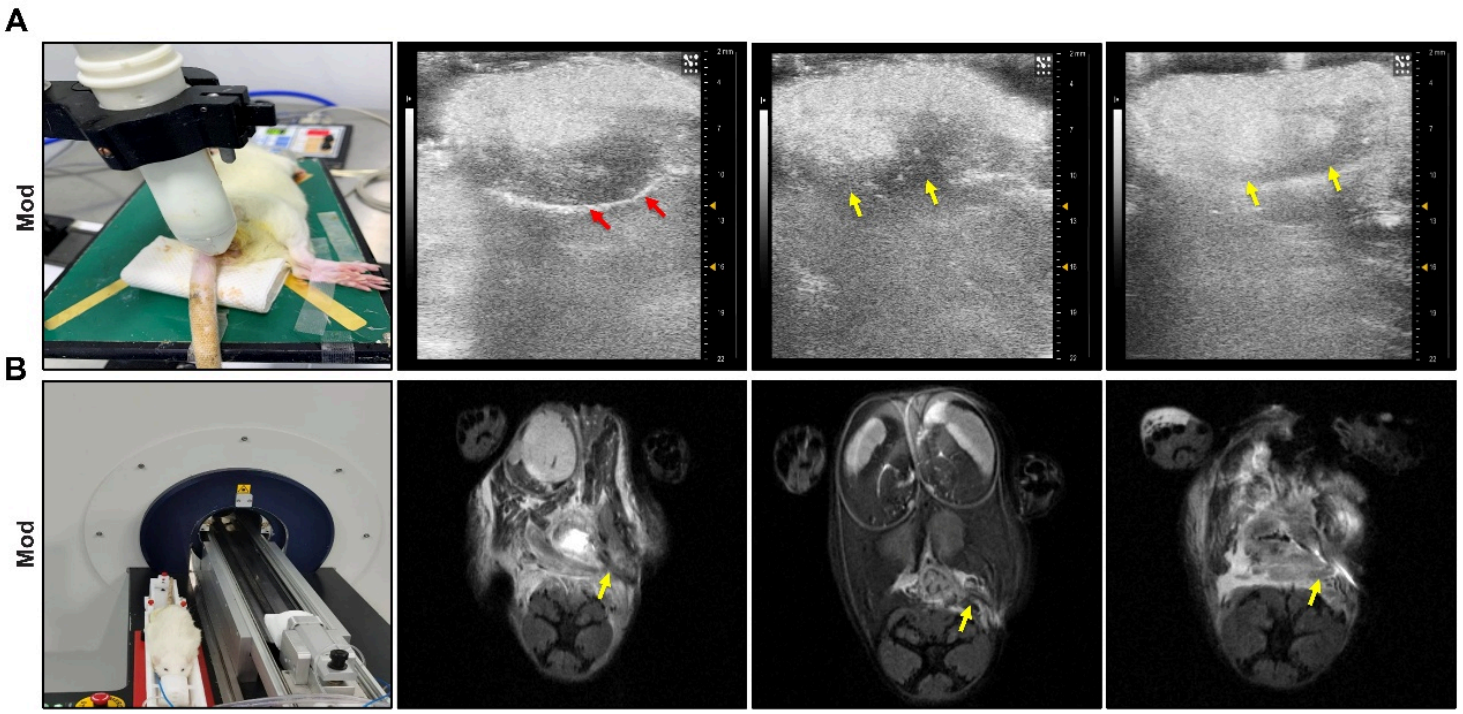


Figure 6

Imaging Evaluation of Perianal Fistulas. A: Perianal ultrasound for evaluating the morphology of the fistula, a steel wire was retained within the perianal region (red arrow); B: Perianal MRI for evaluating the morphology of the fistula.

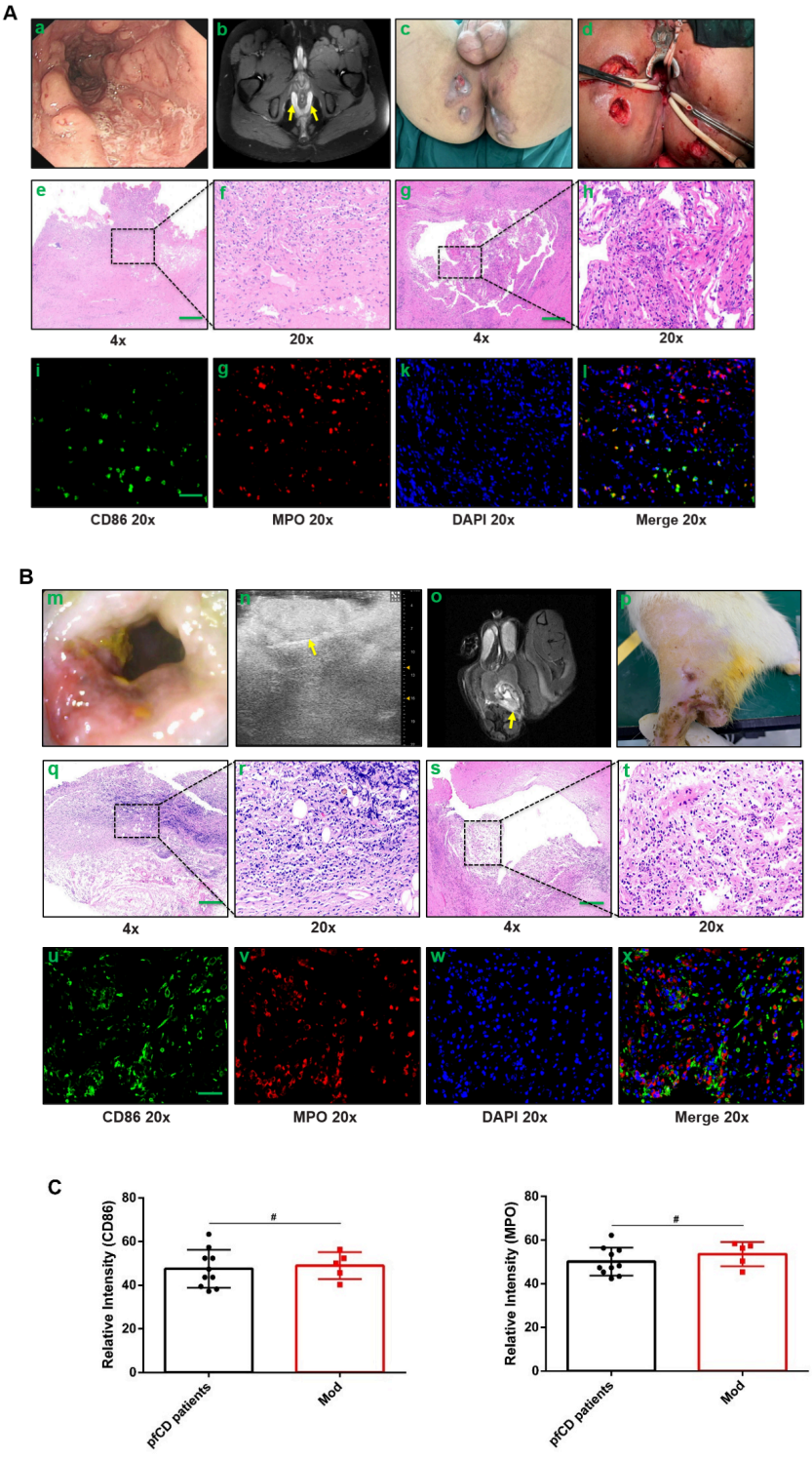


Figure 7

Comparative histopathological and immunofluorescence analysis of perianal fistula tissues from clinical pfCD patients (A) and experimental pfCD rat models (B). (A) Clinical pfCD patient specimens. a: Representative colonoscopic image. b: Perianal MRI (coronal T2WI-fat suppression), with fistula tracts (yellow arrow). c-d: Pre- and post-operative clinical views. e, g: Low-magnification (4×) HE-stained longitudinal and cross-sectional sections of fistula tracts (n=10). Scale bars, 250 μm. f, h: Corresponding higher-magnification (20×) HE views. i-l: Immunofluorescence staining for CD86 (macrophage marker) and MPO (neutrophil marker) in patient fistula tissues (20×). Scale bars, 50 μm. (B) pfCD rat model specimens. a: Colonoscopic findings; b: Perianal ultrasound; c: Perianal MRI; d: Perianal manifestations; q, s: Low-magnification (4×) HE-stained longitudinal and cross-sectional sections of fistula tracts (n=5). Scale bars, 250 μm. r, t: Higher-magnification (20×) HE views. u-x: Immunofluorescence staining for CD86 and MPO in rat model fistula tissues (20×). Scale bars, 50 μm. C: Quantitative analysis of CD86 and MPO. Data were presented as the mean ± SD; $^{\#}P$ 0.05

Supplementary Files

This is a list of supplementary files associated with this preprint. Click to download.

- RevisedWesternblotdescriptionforScientificReports.pdf